

One or more of the Following Statements may affect this Document

- This document has been reproduced from the best copy furnished by the organizational source. It is being released in the interest of making available as much information as possible.
- This document may contain data, which exceeds the sheet parameters. It was furnished in this condition by the organizational source and is the best copy available.
- This document may contain tone-on-tone or color graphs, charts and/or pictures, which have been reproduced in black and white.
- This document is paginated as submitted by the original source.
- Portions of this document are not fully legible due to the historical nature of some of the material. However, it is the best reproduction available from the original submission.

mailed to

X-602-75-121
PREPRINT

NASA TM X-70914

CYCLOTRON SIDE-BAND EMISSIONS FROM MAGNETOSPHERIC ELECTRONS

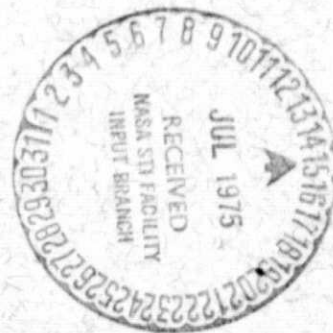
(NASA-TM-X-70914) CYCLOTRON SIDE BAND
EMISSIONS FROM MAGNETOSPHERIC ELECTRONS
(NASA) 19 p HC \$3.25 CSCL 20H

N75-26842

Unclas
G3/73 26640

KAICHI MAEDA

MAY 1975



GODDARD SPACE FLIGHT CENTER
GREENBELT, MARYLAND

X-602-75-121

**CYCLOTRON SIDE-BAND EMISSIONS
FROM MAGNETOSPHERIC ELECTRONS**

**Kaichi Maeda
Theoretical Studies Group**

May 1975

**GODDARD SPACE FLIGHT CENTER
Greenbelt, Maryland**

CYCLOTRON SIDE-BAND EMISSIONS FROM MAGNETOSPHERIC ELECTRONS

Kaichi Maeda
Theoretical Studies Group

ABSTRACT

VLF-emissions with subharmonic cyclotron frequency from magnetospheric electrons have been detected by the S³-A satellite (Explorer 45) whose orbit is close to the magnetic equatorial plane where the wave-particle interaction is most efficient. These emissions were observed during the main phase of a geomagnetic storm in the nightside of the magnetosphere outside of the plasmasphere around $L = 3 \sim 5$. During the event of these side-band emissions, the pitch angle distributions of high energy electrons (>50 keV) and of energetic protons (>100 keV) showed remarkable changes with time, whereas those of low energy electrons and protons remained approximately isotropic. In this type of event, emissions consist essentially of two bands, the one below the equatorial electron gyrofrequency, f_{Ho} , and the other above f_{Ho} . The emissions below f_{Ho} are whistler mode and there is a sharp band of "missing emissions" along $f = f_{Ho}/2$. The emissions above f_{Ho} are electrostatic mode and the frequency ranges up to $3f_{Ho}/2$. It is found that these emissions are generated by the enhanced electron stream penetrating into the nightside magnetosphere during the main phase of a magnetic storm.

CONTENTS

	<u>Page</u>
1. INTRODUCTION	1
2. INSTRUMENTATIONS	1
3. OBSERVATIONS	2
3.1 VLF-Emissions	2
3.2 Electrons	6
3.3 Protons	6
4. DISCUSSIONS	8
ACKNOWLEDGEMENTS	16
REFERENCES	17

ILLUSTRATIONS

<u>Figure</u>		<u>Page</u>
1	A part of the VLF-emission event observed by the S ³ -A satellite on December 17, 1971, for the period from 20 ^h to 21 ^h UT. The upper and the lower figures indicate the emissions of the AC-magnetic field ($f < 3$ kHz) and of the AC-electric field ($f < 10$ kHz), respectively. (Disappearances of the emission at several locations are mostly due to the AGC of the detector.)	3
2	The orbit, No. 101, of the S ³ -A satellite and the locations of VLF-emission events observed on December 17, 1971, which are indicated by a hatched band along the orbit. Two short lines, P. P., indicate approximate positions of the plasmopause. Three lines, A, B and C indicate the locations where the pitch angle distributions of electrons shown in Figure 4 are observed	4

PRECEDING PAGE BLANK NOT FILMED

ILLUSTRATIONS (Continued)

<u>Figure</u>		<u>Page</u>
3	The distribution of frequency, f (in kHz), of VLF-emissions observed by the S ³ -A satellite during the magnetic storm on December 17, 1971, plotted against the local cyclotron frequency of electrons, f_H (in kHz), along the orbit. Vertical dashed lines and full lines indicate the range of frequencies in magnetic field ($f = f_m$) and in electric field ($f = f_E$), corresponding to the emissions shown in the upper and the lower parts of Figure 1, respectively.	5
4	Pitch angle distributions of electron cones at three locations shown in Figure 1. The time corresponding to the locations are A, 20 ^h 10 ^m UT; B, 20 ^h 40 ^m UT and C, 21 ^h 20 ^m UT, respectively. The vertical scale (in logarithmic) is $j(\alpha)/j_0$, where α is the pitch angle and j_0 is a constant (common for all curves).	7
5	Temporal variations of differential intensities of electrons with 90° pitch angle (full lines, $j_{\perp}(E)$, and with the smallest pitch angle (20°, dashed lines), $j_{\parallel}(E)$ respectively, where energies (the median energy, E) are from the top 2, 3, 4, 6, 50, 100, 200 and 400 keV, respectively. Two curves at the bottom are the powers of the differential energy spectra, γ_{\perp} and γ_{\parallel} , determined by the mean value between 3 keV and 400 keV, i. e., $j_{\perp}(E) \propto E^{\gamma_{\perp}}$ and $j_{\parallel}(E) \propto E^{\gamma_{\parallel}}$, respectively. . .	9
6	(a) A schematic plot of the whistler mode emissions based on the combination of the theoretical studies by Matsumoto and Kimura (1971) and by Denavit and Sudan (1973). (b) The growth rate of emissions corresponding to time variation shown in (a), which presents the frequency dependence of the wave generation and attenuation.	15

TABLES

<u>Table</u>		<u>Page</u>
1	Characteristics of the Detectors and Provided Data	2
2	The Mean Energy, E , the Width of Energy Spread in the Measurement, ΔE and the Detector	8
3	Intensity, j_R ($\text{cm}^{-2} \text{sec}^{-1} \text{str}^{-1} \text{keV}^{-1}$), and Kinetic Energy, E_R (in keV), of Electrons in Resonance with Whistler Mode Waves (f/f_H) at Locations A, B, and C Shown in Figure 2	14

CYCLOTRON SIDE-BAND EMISSIONS FROM MAGNETOSPHERIC ELECTRONS

1. INTRODUCTION

The interaction between whistler mode waves and electrons in the magnetosphere is most efficient in the vicinity of the magnetic equator where the wave propagation velocity and its variation along the path of propagation are smallest, corresponding to the minimum of the magnetic field intensity and of its gradient around the equator.

Since the orbit of the S³-A satellite (Explorer 45), whose initial apogee, perigee and inclination are 5.24 R_e, 222 km and 3.6°, respectively, is close to the earth's equatorial plane, the simultaneous observations of VLF-emissions and energetic electrons by this satellite are particularly favorable for studies of wave-particle interactions in the magnetosphere (Longanecker and Hoffman, 1973).

VLF-experiments by satellite were first studied by Dunckel and Helliwell (1969), who have shown by analyzing the OGO-1 data that the source of whistler mode emissions in the magnetosphere lies close to the equatorial plane. This conclusion was based on their finding that the upper frequency limit was proportional to the minimum electron gyrofrequency along the field line passing through the satellite, f_{H0} , the cyclotron frequency at the equator rather than to the local gyrofrequency. The dominant wave generation in the equatorial regions of the earth's magnetosphere has been also discussed by Russell and Holzer (1970). Recently, Tsurutani and Smith (1974) showed the equatorial enhancement of whistler mode wave emissions by investigating the ELF-data obtained by OGO-5.

These previous investigations were limited only to wave data. Although the wave-particle interactions as the cause of these emissions were extensively discussed in these papers, the behavior of particles (especially those of energetic electrons) were left for speculation. In the present study, however, in situ particle observations are available and the temporal variations of electrons, specifically those of energy spectra and of pitch angle distributions during the VLF-events observed by S³-A satellite are discussed. As a preliminary study of this subject, the event which took place during the magnetic storm on December 17, 1971 (Orbit No. 101) is discussed in this paper.

2. INSTRUMENTATIONS

The characteristics of the detectors and of the data obtained by these detectors are listed in Table 1. The details have been described by each experimenter in the references indicated in the table.

Table 1

Characteristics of the Detectors and Provided Data

Data	Characteristic Range	Detector and Reference
Electrons	800 eV to 25 keV	Channel Multiplier (i)
Protons	800 eV to 25 eV	Channel Multiplier (i)
Protons	24 keV to 1.5 MeV	Solid State Detector (ii)
DC Magnetic Field		3-axis Fluxgate Magnetometer (iii)
AC Magnetic Field	1 to 3000 Hz	Search Coil Magnetometer (iv)
AC Electric Field	35 Hz to 100 kHz	Wide Band AGC Receiver (v)
Reference (i) Longanecker and Hoffman, 1973 (ii) Williams, Fritz and Konradi, 1973 (iii) Cahill, 1973 (iv) Parady and Cahill, 1973 (v) Anderson and Gurnett, 1973		

3. OBSERVATIONS

3.1 VLF-EMISSIONS

The event of VLF-emissions in the present investigation was observed for nearly two hours from 20:00 UT to 22:00 UT, which covers the period from the maximum of the main phase to the recovery phase of the December 17 magnetic storm in 1971 (Cahill, 1973). The main portion of the record from 20:00 UT to 21:00 UT is shown in Figure 1. The upper and the lower figure indicate the record of the AC-magnetic field measured by the search coil magnetometer (Parady and Cahill, 1973) and the AC electric field measured by the wide-band recorder (Anderson and Gurnett, 1973), respectively. Locations of these emissions observed by the S³-A satellite are shown by a hatched band along the Orbit No. 101 in Figure 2. Two short lines, P. P. in this figure indicate approximated positions of the plasmapause (Maynard and Cauffman, 1973). As can be seen from the figure, the VLF-emission occurs outside of the plasmasphere in the nightside of the magnetosphere during the period of high geomagnetic activity.

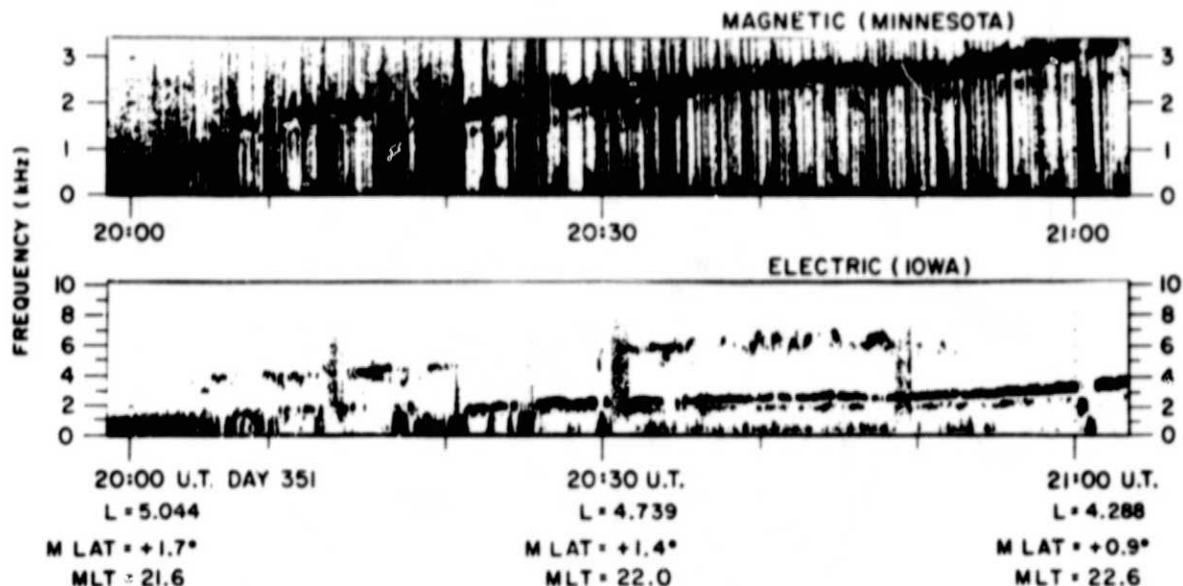


Figure 1. A part of the VLF-emission event observed by the S³-A satellite on December 17, 1971, for the period from 20^h to 21^h UT. The upper and the lower figures indicate the emissions of the AC-magnetic field ($f < 3$ kHz) and of the AC-electric field ($f < 10$ kHz), respectively. (Disappearances of the emission at several locations are mostly due to the AGC of the detector.)

Another significant characteristic of these emissions is the distribution of emitted wave frequencies, f , which consists essentially of two bands, i. e., $f < f_H$ and $f_H < f < 3f_H/2$. This is shown in Figure 3, where the observed frequency, f (in kHz), is plotted against the electron cyclotron frequency, f_H (in kHz). (f_H is obtained from the observed magnetic field intensity along the orbit.) Since the orbit is close to the geomagnetic equatorial plane (the maximum geomagnetic latitude during the event was 5.1° at 2000 UT, Cabill, 1973), f_H can be regarded as the minimum electron-gyrofrequency, f_{Hc} , along the field line which passed through the location of the satellite at the time of the emission event. The vertical dashed lines and full lines in Figure 3 indicate the approximate frequency ranges of the magnetic ($f = f_H$) and electric ($f = f_E$) emission components corresponding to those shown in Figure 1.

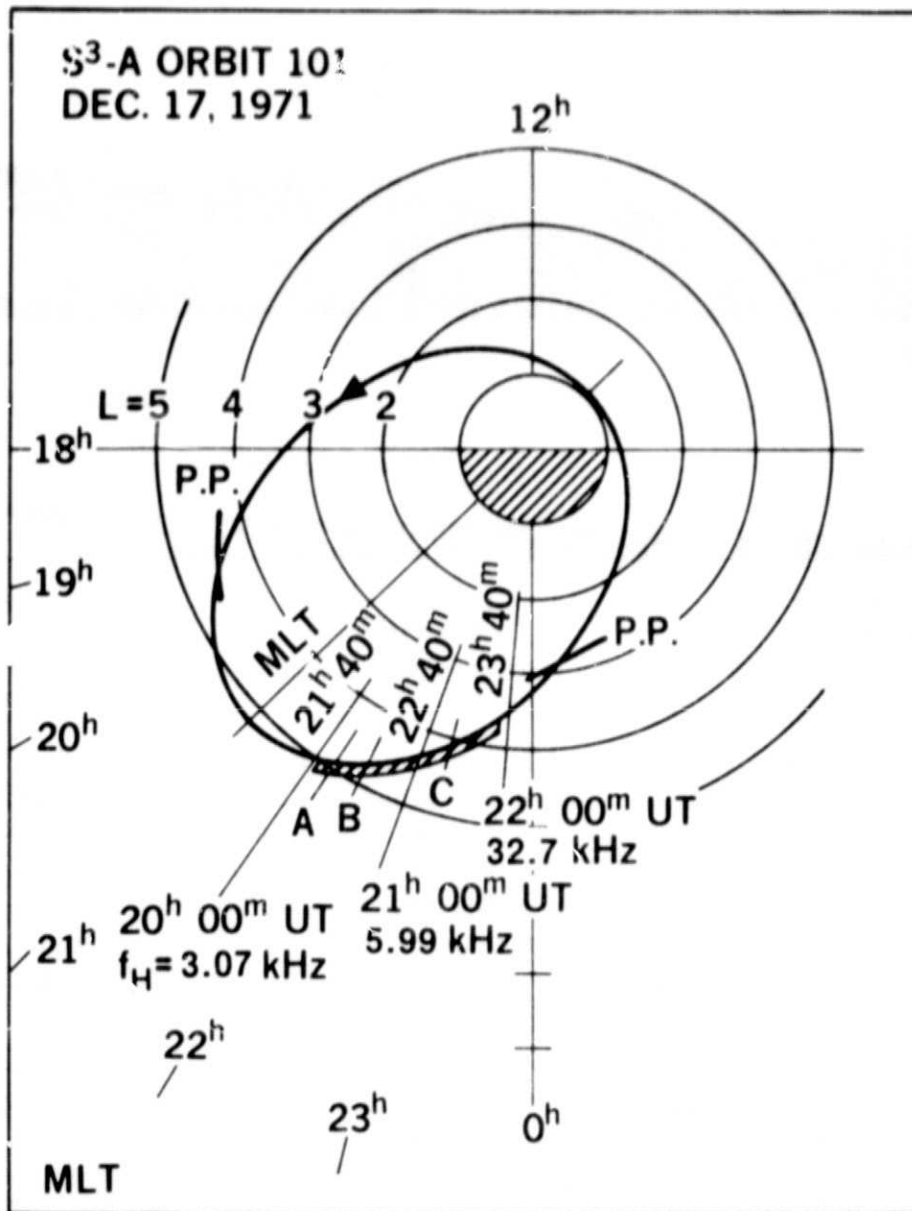


Figure 2. The orbit, No. 101, of the S³-A satellite and the locations of VLF-emission events observed on December 17, 1971, which are indicated by a hatched band along the orbit. Two short lines, P. P., indicate approximate positions of the plasmapause. Three lines, A, B and C indicate the locations where the pitch angle distributions of electrons shown in Figure 4 are observed.

S³-A ORBIT 101, DEC. 17, 1971
(UT 20^h - 22^h)

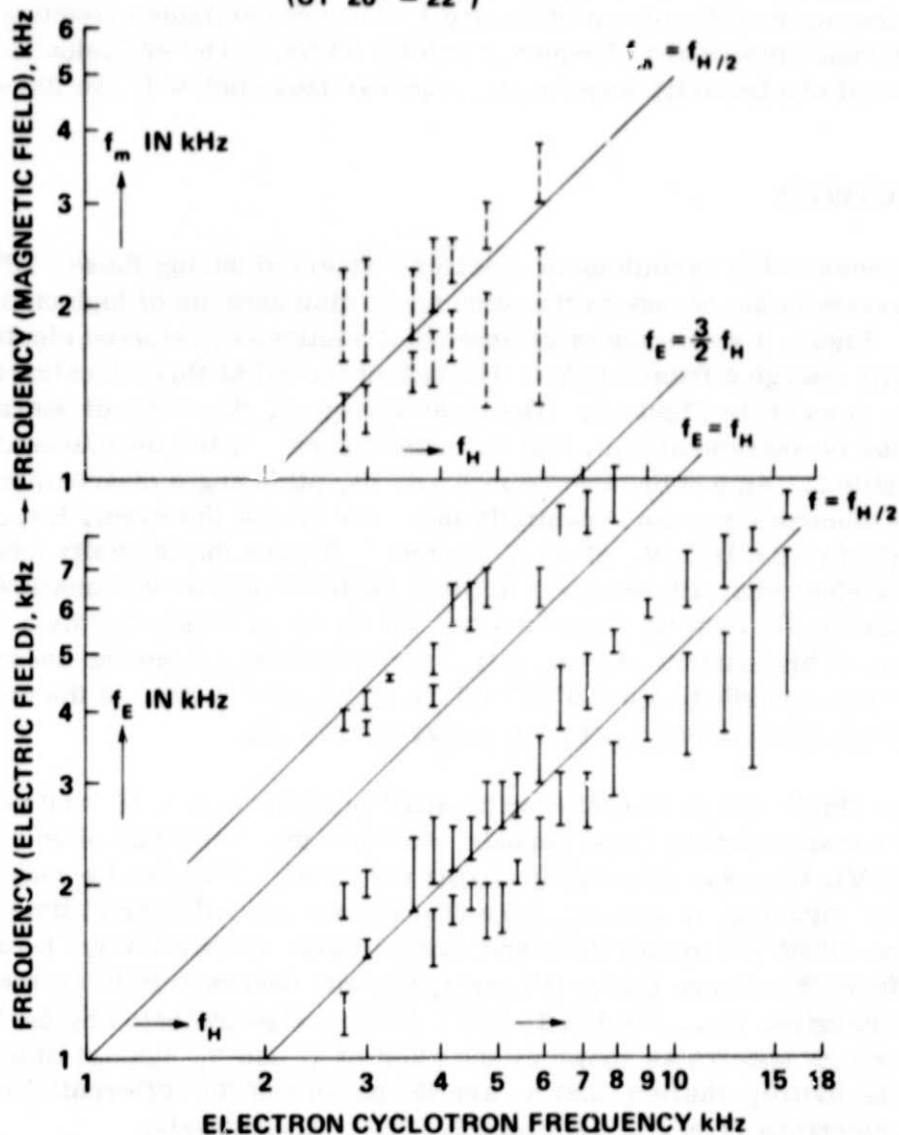


Figure 3. The distribution of frequency, f (in kHz), of VLF-emissions observed by the S³-A satellite during the magnetic storm on December 17, 1971, plotted against the local cyclotron frequency of electrons, f_H (in kHz), along the orbit. Vertical dashed lines and full lines indicate the range of frequencies in magnetic field ($f = f_m$) and in electric field ($f = f_E$), corresponding to the emissions shown in the upper and the lower parts of Figure 1, respectively.

The emissions with frequencies larger than f_{H1} are detected only by the electric field measurement. (This conclusion is based on inspection of the original data corresponding to the left portion of Figure 1 where the emission frequency is below the magnetometer high-frequency cutoff, 3 kHz.) The emission above f_{H1} is therefore of electrostatic wave mode, whereas those below f_{H1} are the whistler mode.

3.2 ELECTRONS

One of the remarkable variations of electrons observed during these VLF-emission events is the change in the pitch angle distributions of high energy electrons. Figure 4 shows the pitch angle distributions of selected electron channels with energies from 2 keV to 400 keV observed at three locations indicated by A, B and C in Figure 2. The mean energy E , the width of energy spread in the measurement, ΔE , and the detector making the measurement are listed in Table 2. As can be seen from Figure 4, pitch angle distributions of low energy electrons remain essentially the same during the event, i. e., $j_{\perp}(E) > j_{\parallel}(E)$ for $E < 10$ keV, where $j_{\perp}(E)$ and $j_{\parallel}(E)$ are the intensity (counts per sec.) of electrons with energy E at pitch angle 90° and at the smallest observable pitch angle ($\sim 20^{\circ}$), respectively. On the other hand, the pitch angle distributions of high energy electrons ($E \geq 50$ keV) change from the so-called "butterfly" type distribution at $20^{\text{h}}10^{\text{m}}$ UT, i. e., $j_{\perp}(E) < j_{\parallel}(E)$, to the normal loss-cone type distribution, $j_{\perp}(E) > j_{\parallel}(E)$ at $21^{\text{h}}20^{\text{m}}$ UT.

Intensities of high energy electrons with small pitch angles, $j_{\parallel}(E \geq 50 \text{ keV})$, are nearly constant during these periods, whereas those of large pitch angle, $j_{\perp}(E \geq 50 \text{ keV})$, increase drastically during the event. This can be seen more clearly from Figure 5, in which $j_{\perp}(E)$ and $j_{\parallel}(E)$ are plotted against time from $20^{\text{h}}00^{\text{m}}$ UT to $21^{\text{h}}30^{\text{m}}$ UT by full lines and dashed lines, respectively. It can be seen also from this figure that $j_{\perp}(E)$ and $j_{\parallel}(E)$ both decrease in the same period at the low energies, i. e., for $E \leq 10$ keV. This is also indicated by the hardening of the energy spectra as shown by the plots of γ_{\perp} and γ_{\parallel} against time in the bottom of the figure, where γ_{\perp} and γ_{\parallel} are the powers of the differential energy spectra of electrons, i. e., $j_{\perp} \propto E^{\gamma_{\perp}}$ and $j_{\parallel} \propto E^{\gamma_{\parallel}}$, respectively.

3.3 PROTONS

Temporal variations of the pitch angle distributions and the intensities of protons (1 - 139 keV) observed by the S³-A satellite during the magnetic storm of December 17, 1971, have been investigated and reported in detail by Williams and Lyons (1974a, b). As can be seen from Figure 4 in their paper (Williams and Lyons, 1974b), the pitch angle distributions of protons from 1 keV to 340 keV are flat-topped, but occasionally concave at 90° at the time of VLF-emission

ELECTRON PITCH ANGLE DISTRIBUTIONS

S³-A ORBIT 101, DEC. 17, 1971

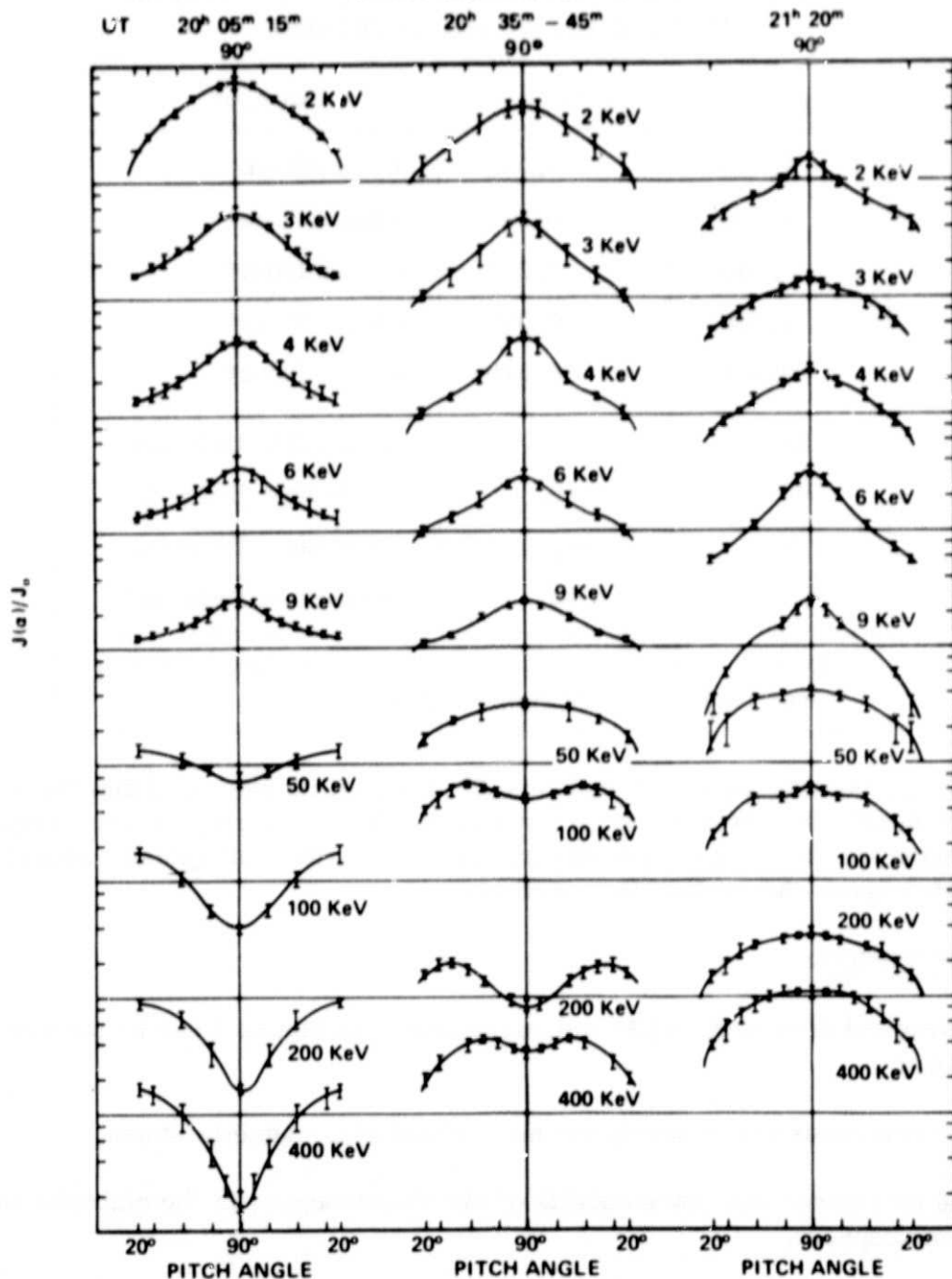


Figure 4. Pitch angle distributions of electron cones at three locations shown in Figure 1. The time corresponding to the locations are A, 20^h10^m UT; B, 20^h40^m UT and C, 21^h20^m UT, respectively. The vertical scale (in logarithmic) is $j(\alpha)/j_0$, where α is the pitch angle and j_0 is a constant (common for all curves).

Table 2

The Mean Energy, E, the Width of Energy Spread in the Measurement, ΔE and the Detector

E (in keV)	ΔE (in keV)	Detector
1.760	0.546	Channeltron*
2.694	0.835	Channeltron*
4.040	1.252	Channeltron*
6.040	1.872	Channeltron*
9.160	2.840	Channeltron*
55.	38.	Solid-State Detector
105.	49.	Solid-State Detector
188.	104.	Solid-State Detector
325.	125.	Solid-State Detector

*During orbit No. 101, this detector was not operating over its full energy range 1.2 to 25 keV.

event (i.e., in bound Orbit 101 at $L = 5.2 \sim 4.7$). It is concluded that these protons are mainly the ring current protons in the strongly turbulent outer region of the magnetosphere where the plasma from the earth's tail (plasma sheet) has penetrated inside the orbit of the satellite.

4. DISCUSSIONS

The characteristics of the VLF-emissions shown in Figure 1 can be summarized as follows:

- (i) The emissions occur during the main phase of a magnetic storm.
- (ii) The emissions take place outside of the plasmasphere in the nightside of the magnetosphere.
- (iii) The emissions consist of the following three significant frequency regimes: (a) $f < f_{Ho}/2$, (b) $f \gtrsim f_{Ho}/2$ and (c) $f \lesssim 3f_{Ho}/2$ where f_{Ho} is the electron cyclotron frequency at the magnetic equator.

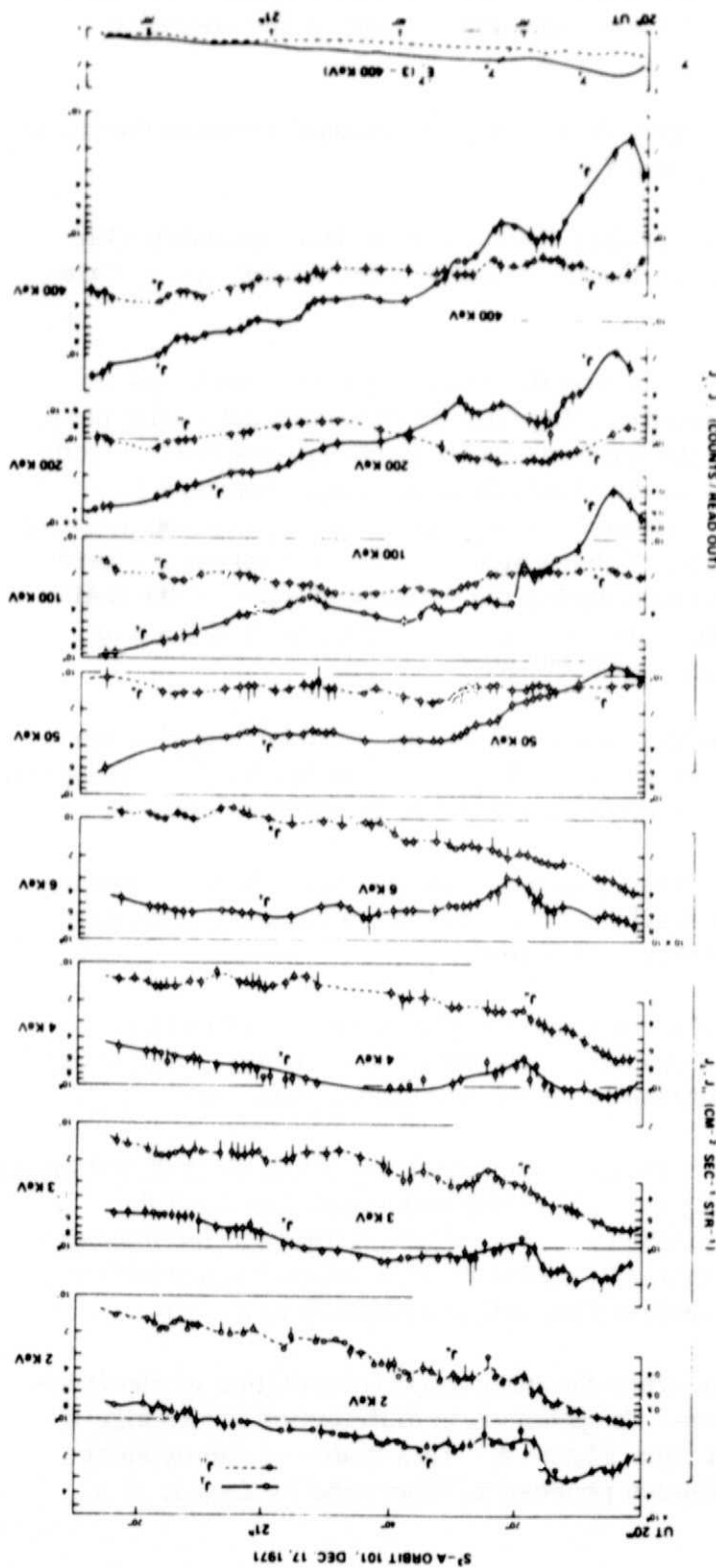


Figure 5. Temporal variations of differential intensities of electrons with 90° pitch angle (full lines, $j_{\perp}(E)$), and with the smallest pitch angle (20°, dashed lines), $j_{\parallel}(E)$ respectively, where energies (the median energy, E) are from the top 2, 3, 4, 6, 50, 100, 200 and 400 keV, respectively. Two curves at the bottom are the powers of the differential energy spectra, γ_{\perp} and γ_{\parallel} , determined by the mean value between 3 keV and 400 keV, i. e., $j_{\perp}(E) \propto E^{-\gamma_{\perp}}$ and $j_{\parallel}(E) \propto E^{-\gamma_{\parallel}}$, respectively.

Emissions of regimes (a) and (b) are whistler mode waves, whereas emissions of regime (c) are electrostatic mode, corresponding to one of the so-called Bernstein mode waves.

(iv) Subsequently, there are two bands of "missing emissions" between the three bands of emissions, i. e., $f \approx f_{Ho}/2$ and $f \approx f_{Ho}$.

(v) Although the intensity of the emissions fluctuate with time, possibly with some fine structures, the duration of the whole event is very long, i. e., more than two hours.

The characteristics (i) and (ii) indicate that the source of these emissions is linked to the particles in the asymmetric ring current developing the main phase of the magnetic storm. Possibly the VLF-producing particles are the energetic electrons which have penetrated into the nightside of the magnetosphere from the plasma sheet and are drifting eastwards after encountering the steep gradient of the earth's magnetic field. Entry of these electrons into the magnetosphere is associated with ring current protons during the developing stage of the main phase of the magnetic storm. Those protons carry the most part of the ring current energy (Smith and Hoffman, 1973, 1974).

Since the pitch angle variations of high energy electrons (>50 keV) during the emission event are quite drastic (as shown in Figures 4 and 5), the VLF-emission mechanism and its energy should be directly related to energetic electrons.

To consider the relation between the emission and the particles in the magnetosphere during these events, the behavior of electrons and protons observed by the satellite will be worth summarizing as follows:

(1) The pitch angle distribution of the low energy electrons ($1 \sim 10$ keV) in the asymmetric ring current does not change during the event. It stays essentially in the normal rounded top type distribution with an intensity maximum at 90° .

(2) As the VLF-emission event progresses with time, the pitch angle distributions of high energy electrons (>50 keV) indicate remarkable variation from the butterfly type (with the intensity minimum at $\alpha = 90^\circ$ comparable to the intensity inside the loss-cone, leaving an intensity maximum somewhere around 20° or less) to the normal rounded type distribution with a maximum at $\alpha = 90^\circ$.

(3) In the later stage of emission, when the pitch angle distribution of electrons approaches the normal rounded type, the pitch angle distribution shows significant "shoulders," as can be seen from Figure 4. This indicates the existence of the two types of pitch angle diffusion process as discussed by Lyons, et al.

(1971, 1972), i. e., the one acting effectively near $\alpha = 90^\circ$ (the Landau resonance), and the other is most effective in the smaller pitch angles (the cyclotron resonances). The shoulder in the electron pitch angle distribution corresponds to the angular regime of weak diffusion between these two pitch angle regimes of strong diffusion. The details of electron pitch angle distributions observed by the S³-A satellite and its theoretical interpretations were discussed recently by Lyons and Williams (1975).

(4) The intensity of low energy electrons (< 10 keV) decreases slowly with time during the event. As can be seen from Figure 5, the rate of decrease is larger for the component with small pitch-angle, j_{\parallel} , than for the large pitch angle component, j_{\perp} .

(5) On the other hand, the intensity of high energy (> 50 keV) electrons with large pitch-angle, j_{\perp} , shows a remarkable increase with time during the event, while that of small-pitch angles, j_{\parallel} , stays relatively constant. In the later stage of the event, j_{\parallel} of high energy electrons also increases slightly, as can be seen from Figure 5.

(6) Corresponding to the different trends with time in high energy electrons and in low energy electrons described above in (4) and (5), the electron energy spectrum of these electrons becomes harder as the VLF-event progresses. This is shown by the decrease of γ_{\perp} and γ_{\parallel} with time, as plotted in the bottom of Figure 5. Due to the drastic increase of high energy electrons of $\alpha = 90^\circ$ component, the rate of decrease of γ_{\perp} is larger than that of γ_{\parallel} .

It should be noted that the observation of these time variations of the VLF-emissions and of the electrons is made by the satellite along its inbound orbit, as shown in Figure 2. The hardening of the energy spectrum of electrons is, therefore, essentially due to the inward cross-magnetic diffusion of those geomagnetically trapped electrons. In other words, the satellite is observing essentially the same group of ring current electrons at different locations in the magnetosphere, i. e., the hardening of the energy spectrum of electrons particularly those of large pitch angle component is mainly spatial rather than temporal. It should be also noted that the shift of the VLF-emission frequency to higher frequency (as shown in Figure 1) is a spatial effect, due to the increase of the magnetic field as the satellite moves toward the earth.

(7) Since the magnetic storm time variation of protons on December 17, 1971, in the nightside of the magnetosphere has been investigated in detail by Smith and Hoffman (1973) and by Williams and Lyons (1974a, b), the variation of protons during the VLF-event (20 - 22 UT on December 17, 1971) can be examined from their results.

According to Williams and Lyons (1974a, b), the pitch angle distribution of protons does not indicate drastic change as occurred in that of electrons.

One of the peculiar features of the VLF-emissions is the existence of two bands of "missing emissions" (as shown in Figure 1). This was also observed outside the plasmasphere in the nightside near the equatorial plane during other magnetic storms, by triaxial magnetic sensors on the OGO-5 satellite (Tsurutani and Smith, 1974). Since the frequency range observed by OGO-5 was 1500 - 10 Hz, corresponding to $L = 5 \sim 10$, the emissions are called post-midnight ELF-chorus. Tsurutani and Smith speculate that these ELF-emissions are generated by energetic electrons (>40 keV) injected into the midnight sector during a magnetospheric substorm, interacting with whistler mode waves around the equator. The extinction of the emission in the frequency band near $0.5f_{H_0}$ is considered to be due to Landau damping. Particles in cyclotron resonance with waves for which $f = f_{H_0}/2$ have a parallel velocity $V_{\parallel} = V_{ph}$, where V_{ph} is the phase velocity of the wave. Thus it is concluded that electrons travelling opposite to the waves and in cyclotron resonance with them at this frequency, i. e., $f = f_{H_0}/2$, will cause wave growth, whereas particles with the same V_{\parallel} but travelling in the same direction as the waves will cause wave damping (Tsurutani and Smith, 1974).

Burtis and Helliwell (1969) detected similar VLF-emissions, using the magnetic loop antenna on the OGO-1 and 3 spacecrafts. They concluded that the half-gyrofrequency effect is related to the topological change in the refractive index surface that occurs at half the electron gyrofrequency, i. e., the propagation effect. Although Burtis and Helliwell did not discuss the extinction band at $f_{H_0}/2$ in their results, the existence of this kind of missing emission band is also clear from Figure 3 of their paper in the frequency range 7 - 20 kHz. In this plotting, they used the Williams and Mead (1965) magnetospheric model. If the magnetic field intensity measured by the on-board sensors is used, the band of missing emission at $f_{H_0}/2$ might have been seen even below 6 kHz in their results.

Now, let us examine the energies of electrons interacting with Doppler-shifted whistler waves. The kinetic energy of resonant electrons, $E_R \simeq \frac{m_e}{2} V_R^2$, can be obtained as a function of wave frequency by eliminating the wave number, k_{\parallel} , from the resonance condition

$$\omega - k_{\parallel} V_R = n\Omega_e, \quad (n = 1, 2, \dots) \quad (4.1)$$

and the dispersion formula of the wave propagating parallel to the magnetic field

$$\frac{k_{\perp}^2 c^2}{\omega^2} \cong \frac{\omega_p^2}{\omega(\Omega_e - \omega)} \quad (4.2)$$

giving,

$$E_R = \frac{m_e c^2}{2} \cdot \frac{|\Omega_e - \omega|^3}{\omega_p^2 \omega} \quad (\text{for } n = 1). \quad (4.3)$$

where $m_e c^2 \cong 500$ keV, the plasma frequency, ω_p , must be assumed since the plasma density is not measured by the S³-A on-board detector whereas the electron gyrofrequency, Ω_e , can be accurately calculated by using the total magnetic field intensity measured by the on-board magnetometers.

The energies of electrons in resonance with whistler mode waves of frequencies around half gyrofrequency of electron, i. e., $f/f_H = 0.4, 0.5$ and 0.6 , at three locations, A, B and C shown in Figure 2, are listed in Table 3 for two values of assumed plasma densities, $N_e = 10$ and 1 cm^{-3} , respectively. Since the energies of electrons in resonant with whistler mode waves changes approximately from 1 keV at 20^h UT to 100 keV at 21^h UT as shown in Table 3, Figure 5 indicates that these whistler mode emissions are caused by the enhancement of the corresponding energetic electrons at each location in the magnetosphere. Thus, the variations of electrons and of VLF-emissions are from spatial distributions rather than the temporal variation.

In the upper part (a) of Figure 6, a schematic expression of VLF-emissions and their damping based on the combination of two theoretical studies is presented. The emissions of frequencies $f \sim f_H/2$ are generated by the instabilities of 'triple-structure' loss cone type electron pitch angle distributions of electrons, which consist of thermal (2 - 5 eV), quasithermal (10 - 50 eV) and transient beam electrons (100 eV) as given by Matsumoto and Kimura (1971). The calculation on these instabilities are extended from the linear theory to the non-linear numerical simulations. As shown in the lower part (b) of the figure, the non-linear growth rate reduces the growth rate given by the linear theory beyond the characteristic growth time. In the non-linear theory, the frequency of maximum growth rate shifts towards higher frequency. This is, however, negligibly small to be shown in the figure. The emission below the half electron gyrofrequency indicated in Figure 6(a) is due to the non-linear theory by Sudan and Ott (1971), assuming the energy of beam electrons to be 50 keV. In this schematic expression, an analytic formula derived by Denavit and Sudan (1973) is actually used simply to show the frequency dependence of the growth rate. In general the frequency range near the electron cyclotron frequency, f_{HP} is hard to excite unless a very large anisotropy exists in the pitch angle distribution.

Table 3

Intensity, j_R ($\text{cm}^{-2} \text{sec}^{-1} \text{str}^{-1} \text{keV}^{-1}$), and Kinetic Energy, E_R (in keV), of Electrons in Resonance with Whistler Mode Waves (f/f_H) at Locations A, B, and C Shown in Figure 2

f_H (kHz)	A 2.88		B 3.89		C 21.6	
(i) If $N_e \simeq 10/\text{cc}$	E_R	j_R	E_R	j_R	E_R	j_R
$f/f_H = 0.4$	1.8	2×10^9	2.9	1.1×10^9	100	5×10^5
0.5	0.9	$> 2 \times 10^9$	1.5	$> 1.2 \times 10^9$	58	5.4×10^5
0.6		$> 2 \times 10^9$	0.6	$> 1.2 \times 10^9$	18	($\gtrsim 10^6$)
(ii) If $N_e \simeq 1/\text{cc}$						
$f/f_H = 0.4$	18	($\gtrsim 10^6$)	(30	$\gtrsim 10^6$)	1000	-
0.5	9	5×10^8	15	$\sim 10^8$	580	$\gtrsim 10^3$
0.6	3	7×10^8	6	4.3×10^8	180	8×10^4

It should also be noted that the non-linear theory by Sudan and Ott (1971) as well as by Denavit and Sudan (1973) are based on the narrow band approximation. In this respect, it is questionable to apply the theory of Sudan and Ott (1971) to the present problem of the broadband whistler mode noise interacting with electrons of wide-range distributions.

Furthermore, the gap of missing emissions at $f_H/2$ shown in Figure 6(a) is too wide as compared with the observed gap shown in Figure 1. Although this gap of missing emissions widens with increasing frequency (see Figure 1), other mechanisms, such as the evanescent mode of beam-wave interaction discussed by Briggs (1969) and by Neufeld and Wright (1963) can be considered as possible sources of this sharp extinction band of emission.

Summarizing the simultaneous measurements of VLF-emission and energetic particles made by the on-board detectors of the S³-A satellite during the main phase of the magnetic storm on December 17, 1971, the following significant points are found: (1) These emissions are related to energetic electrons whose energy spectra and pitch angle distributions indicate remarkable variations during the emission events. (2) The emissions occur outside of the plasma sphere in the nightside magnetosphere where the energetic ring current protons and electrons are drifting from the plasma sheet in the earth's magnetic tail.

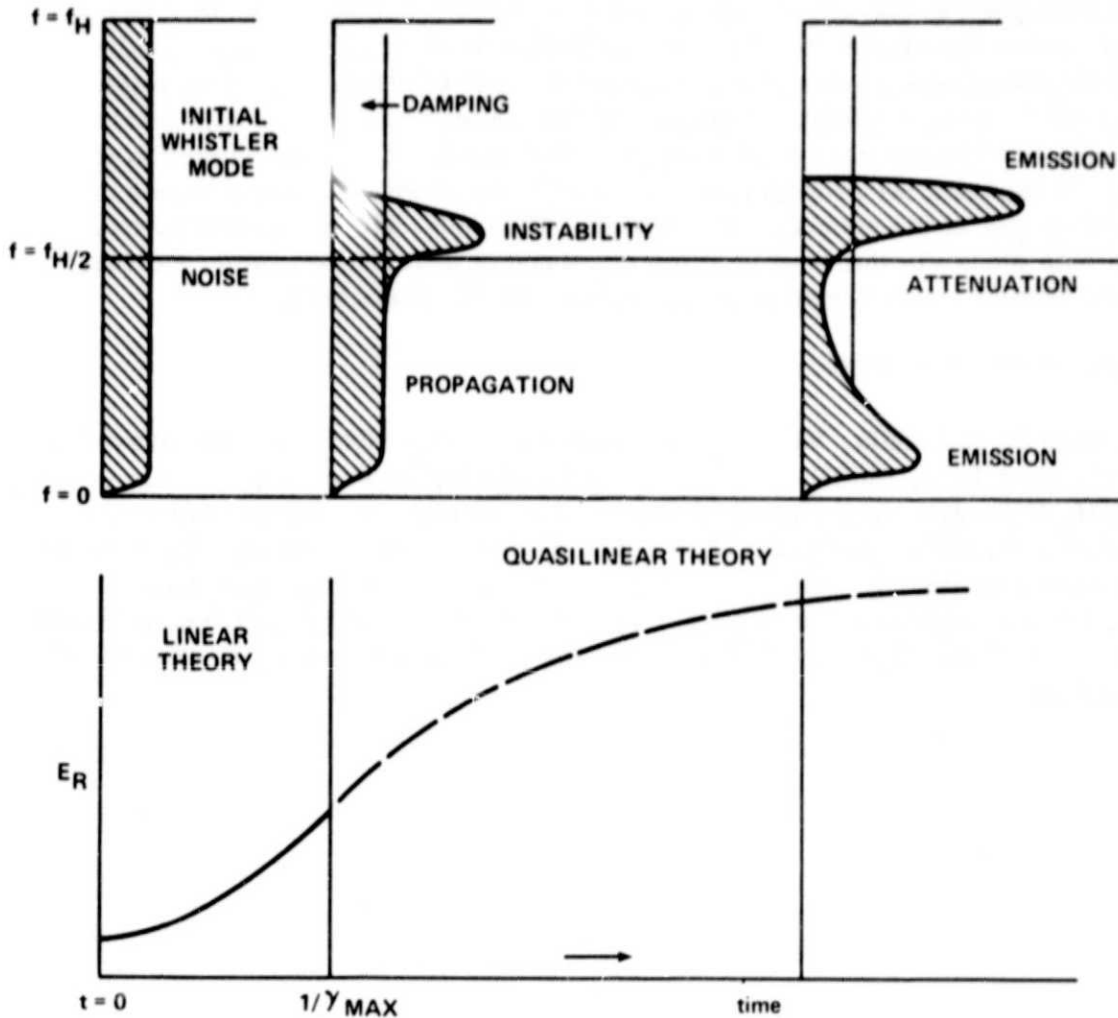


Figure 6. (a) A schematic plot of the whistler mode emissions based on the combination of the theoretical studies by Matsumoto and Kimura (1971) and by Denavit and Sudan (1973). (b) The growth rate of emissions corresponding to time variation shown in (a), which presents the frequency dependence of the wave generation and attenuation.

(3) The emissions consist of whistler mode waves and the electrostatic mode emission. (4) The whistler mode emissions are generated by the instabilities of relatively low energy electrons at $L \gtrsim 4$ (~ 1 keV) with the broadband whistler mode noises in the magnetosphere. Later they shift to higher energies (>100 keV) as L -value decreases. (5) The electrostatic mode emission might be one of the Bernstein mode waves with frequency $f \lesssim 3f_H/2$. These emissions are, however,

not investigated in the present study. (6) The whistler mode emissions have a sharp band of missing emissions (the extinction band) at $f_H/2$. This gap (the extinction band) can be due to the evanescent mode of beam-wave interaction discussed by Briggs (1964). However, if the center frequency of this missing emission band is exactly a half electron gyrofrequency $f_H/2$, the extinction can be due to the peculiar propagation characteristics of whistler mode waves of frequency $f_H/2$ at the geomagnetic equator. This point will be further investigated with other similar events which occurred in different magnetic storms. (7) The role of ring-current protons in these events is unclear.

ACKNOWLEDGEMENTS

AC-magnetic field data, VLF-electric field data and particle data are provided by Professor L. J. Cahill, University of Minnesota, by Professor D. A. Gurnett, University of Iowa and by Dr. R. A. Hoffman, the project scientist of the S³-A satellite, at the Goddard Space Flight Center, respectively, to whom I am very grateful. I would like to thank Roger R. Anderson, University of Iowa, for his cooperation in editing VLF-data for the present study and to Naren Bewtra and Chris Gloeckler of G. S. F. C. for their help in computer analysis of particle data.

REFERENCES

- Anderson, R. R., and Gurnett, D. A., "Plasma Wave Observations near the Plasmapause with the S³-A Satellite," J. Geophys. Res., 4756-4764, 1973.
- Briggs, R. J., "Electron-Stream Interaction with Plasmas," M. I. T. Press, Cambridge, Massachusetts, 1964.
- Burtis, W. J., and Helliwell, R. A., "Banded Chorus - A New Type of VLF Radiation Observed in the Magnetosphere by OGO 1 and OGO 3," J. Geophys. Res., 74, 3002-3010, 1969.
- Cahill, Jr., L. J., "Magnetic Storm Inflation in the Evening Sector," J. Geophys. Res., 78, 4724-4730, 1973.
- Denavit, J., and Sudan, R. N., "Whistler Sideband Instability," Bull. Am. Phys. Soc., 18, 1280, 1973.
- Dunckel, N., and Helliwell, R. A., "Whistler-Mode Emissions on the OGO 1 Satellite," J. Geophys. Res., 74, 6371-6385, 1969.
- Hoffman, R. A., "Particle and Field Observations from Explorer 45 during the December 1971 Magnetic Storm Period," J. Geophys. Res., 78, 4771-4777, 1975.
- Longanecker, G. W., and Hoffman, R. A., "S³-A Spacecraft and Experiment Description," J. Geophys. Res., 78, 4711-4717, 1973.
- Lyons, L. R., and Williams, D. J., "The Quiet Time Structure of Energetic (35-560 keV) Radiation Belt Electrons," J. Geophys. Res., 80, 943-950, 1975.
- Lyons, L. R., Thorne, R. M., and Kennel, C. F., "Electron Pitch-Angle Diffusion Driven by Oblique Whistler-Mode Turbulence," J. Plasma Phys., 6, 589-606, 1971.
- Lyons, L. R., Thorne, R. M., and Kennel, C. F., "Pitch-Angle Diffusion of Radiation Belt Electrons with the Plasmasphere," J. Geophys. Res., 77, 3455-3474, 1972.
- Lyons, L. R., "Electron Diffusion Driven by Magnetospheric Electrostatic Waves," J. Geophys. Res., 79, 575-580, 1974.

- Matsumoto, H., and Kimura, I., "Linear and Nonlinear Cyclotron Instability and VLF Emissions in the Magnetosphere," *Planet. Space Sci.*, 19, 567-608, 1971.
- Maynard, N. C., and Cauffman, D. P., "Double Floating Probe Measurements on S³-A," *J. Geophys. Res.*, 78, 4745-4750, 1973.
- Neufeld, J., and Wright, H., "Instabilities in a Plasma-Beam System Immersed in a Magnetic Field," *Phys. Rev.*, 129, 1489-1507, 1963.
- Parady, B., and Cahill, Jr., L. J., "ELF Observations during the December 1971 Storm," *J. Geophys. Res.*, 78, 4765-4770, 1973.
- Russell, C. T., and Holzer, R. E., "AC Magnetic Fields," in *Particles and Fields in the Magnetosphere*, ed., McCormac, B. M., 195-212, D. Reidel Dordrecht, Netherland, 1970.
- Smith, P. H., and Hoffman, R. A., "Ring Current Particle Distribution during the Magnetic Storms of December 16-18, 1971," *J. Geophys. Res.*, 78, 4731-4737, 1973.
- Smith, P. H., and Hoffman, R. A., "Direct Observations in the Dusk Hours of the Characteristics of the Storm Time Ring Current Particles During the Beginning of Magnetic Storms," *J. Geophys. Res.*, 79, 966-971, 1974.
- Sudan, R. N., and Ott, E., "Theory of Triggered VLF-Emissions," *J. Geophys. Res.*, 76, 4463-4475, 1971.
- Tsurutani, B. T., and E. J. Smith, "Postmidnight Chorus: A Substorm Phenomenon," *J. Geophys. Res.*, 79, 118-127, 1974.
- Williams, D. J., Fritz, T. A., and Konradi, A., "Observations of Proton Spectra ($1.0 < E_p < 300$ keV) and Fluxes at the Plasmapause," *J. Geophys. Res.*, 78, 4751-4755, 1973.
- Williams, D. J., and Lyons, L. R., "The Ring Current and Its Interaction with the Plasmapause Storm Recovery Phase," *J. Geophys. Res.*, 79, 4195-4207, 1974.
- Williams, D. J., and Lyons, L. R., "Further Aspects of the Ring Current Interaction with the Plasmapause: Main and Recovery Phase," *J. Geophys. Res.*, 79, 4791-4798, 1974.

Williams, D. J., and Mead, G. D., "Nightside Magnetosphere Configuration as Observed from Trapped Electrons at 1100 Kilometers," J. Geophys. Res., 70, 3017-3029, 1965.